Rapid fabrication of Al-based bulk-form nanocomposites with novel reinforcement and enhanced performance by selective laser melting

Dongdong Gu,[a,*] Hongqiao Wang,[a] Donghua Dai,[a] Pengpeng Yuan,[a]
Wilhelm Meiners[b] and Reinhart Poprawe[b]

[a]College of Materials Science and Technology, Nanjing University of Aeronautics and Astronautics, Yudao Street 29,
Nanjing 210016, People's Republic of China
[b]Fraunhofer Institute for Laser Technology ILT/Chair for Laser Technology LLT,
RWTH Aachen, Steinbachstraße 15, D-52074 Aachen, Germany

A novel ring-structured nanoscale TiC reinforcement with a regular distribution was tailored along the grain boundaries of the matrix by selective laser melting (SLM) to produce TiC/AlSi10 Mg nanocomposite parts. Relative to the SLM-processed unreinforced AlSi10 Mg part, the TiC/AlSi10 Mg nanocomposite part with the novel reinforcement architecture exhibited elevated microhardness (188.3 $HV_{0.1}$) and tensile strength (486 MPa) without a reduction in elongation (10.9%), due to the combined effects of grain refinement and grain boundary strengthening caused by the ring-structured nanoscale TiC reinforcement.
© 2014 Acta Materialia Inc. Published by Elsevier Ltd. All rights reserved.

As outstanding high-performance lightweight materials, aluminum matrix composites (AMCs) reinforced with harder and stiffer ceramic particles are widely used in aerospace, aircraft and automotive applications because of their excellent properties, such as high specific stiffness, high specific strength and excellent wear resistance [1–4]. Normally, the improvement in the mechanical properties of AMCs is mainly determined by the particle size and distribution state of the reinforcement [5]. It has been found that decreasing the reinforcement particle size from the relatively large micrometer level to the considerably finer nanometer scale can lead to the simultaneous enhancement of the strength and ductility of AMCs [6,7]. Such novel materials are defined as nanocomposites [8]. Currently, several manufacturing techniques are used to produce nanoparticle-reinforced AMCs, including mechanical alloying [9,10], powder metallurgy [11,12], stir-casting [6,7], etc. The aim of these methods is generally to obtain a uniform distribution of nanoscale reinforcing phase in the matrix in order to enhance the reinforcement effect. Differently, some previous research work has revealed that the mechanical properties of metal matrix composites (MMCs) can be further improved by tailoring the distribution of reinforcement on a microscopic level [13,14]. However, previous research efforts have mainly been focused on controlling microstructures of MMCs reinforced with microsized ceramic particles. For ultrafine nanoscale ceramic reinforcement, it is much more difficult to tailor the distribution during MMC preparation: the uncontrolled agglomeration of nanoparticles due to the considerably large van der Waals attractive forces tends to cause significant microstructural inhomogeneity. Very little previous work has been reported on the processing of nanocomposites with novel reinforcement microstructure.

Selective laser melting (SLM) is regarded as a promising additive manufacturing technique due to its flexibility in producing complex shaped parts directly from loose powder [15–17]. SLM provides new technological opportunities for fabricating high-performance MMCs parts with unique microstructures, because of the extremely rapid melting/solidification induced by non-equilibrium laser scanning [18–21]. Very recently, work has been carried out that testifies to the possibility of processing Fe-matrix and Ti-matrix nanocomposites using SLM [16,17]. However, there are no previous reports on SLM processing of Al-based nanocomposite parts with tailored microstructure and performance. This work on SLM of bulk-form TiC/AlSi10 Mg nanocomposites thus concentrates on the above issue. The nanoscale TiC is selected as reinforcement based on its good wettability and thermodynamic stability within the molten aluminum. This work focused on the

* Corresponding author. Tel./fax: +86 25 52112626; e-mail: dongdonggu@nuaa.edu.cn

influence of SLM processing parameters on microstructural evolution and mechanical properties (especially tensile strength and elongation) of SLM-processed Al-based nanocomposites. A process–microstructure–performance relationship was established to enable the successful production of AMC parts with tailored reinforcement architecture and improved mechanical performance.

99.0% purity TiC nanopowder with a non-spherical shape and a mean particle size of 50 nm, and 99.7% purity AlSi10 Mg powder with a spherical shape and an average particle diameter of 30 μm were used. The TiC and AlSi10 Mg powder system consisting of 3 wt.% TiC were mechanically mixed in a Fritsch Pulverisette 4 vario-planetary mill, using a ball-to-powder weight ratio of 1:1, a rotation speed of the main disk of 200 rpm, and a mixing duration of 4 h.

The SLM system consisted mainly of an IPG YLR-200-SM ytterbium fiber laser with a power of $\sim$200 W and a spot size of 70 μm, an automatic powder spreading device, an inert argon gas protection system, and a computer system for process control. Based on a series of preliminary experiments, the following SLM parameters were optimized: scan speed (v) = 200 mm s^{-1}, scan line hatch spacing (h) = 50 μm, and powder layer thickness (d) = 50 μm. In order to change the processing conditions during experiments, various laser powers (P) of 80, 100, 120 and 140 W were set by the SLM control program. Four different "volumetric laser energy densities" (E) of 160, 200, 240 and 280 J mm^{-3}, which were defined by $E = \frac{P}{vhd}$ [22], were used to assess the laser energy input to the powder layer being processed.

Specimens for metallographic examinations were prepared according to standard procedures, and etched with a solution containing HF (2 ml), HCl (3 ml), HNO$_3$ (5 ml) and distilled water (190 ml) for 10 s. High-resolution study of the ultrafine nanostructures of SLM-processed nanocomposite samples was performed by field emission scanning electron microscopy (FE-SEM) using a Hitachi S-4800 at 5 kV. Phase identification was performed by X-ray diffraction (XRD) using a Bruker D8 Advance diffractometer with Cu K_α radiation at 40 kV and 40 mA, using a continuous scan mode at 4° min^{-1}. The Vickers hardness was measured using a MicroMet 5101 microhardness tester at a load of 0.1 kg and an indentation time of 20 s. The SLM-processed samples were cut using a spark-erosion wire cutting machine to prepare standard specimens for tensile tests, according to the standard GB/T228–2010. The tensile direction was parallel to the SLM-processed layers. Uniaxial tensile tests were performed at room temperature with a SANS CMT5105 universal testing machine at a strain rate of 1×10^{-4} s^{-1}. The ultimate tensile strength and elongation were determined from the stress–strain curves.

The characteristic phases and microstructures of the SLM-processed TiC/AlSi10 Mg nanocomposite parts are illustrated in Figs. 1 and 2, showing the different morphologies and distributions of the reinforcement at various laser energy densities (E). As revealed in the XRD pattern of an SLM-processed part (Fig. 1e), strong diffraction peaks corresponding to Al$_9$Si (JCPDS Card No. 65-8554), as the matrix phase, and stoichiometric TiC (JCPDS Card No. 65-8805), as the reinforcing phase, were identified. Energy-dispersive X-ray spectroscopy (EDX) spot scan analysis was also performed on the matrix (Point 1, Fig. 1c) and the reinforcement (Point 2) to identify quantitatively the chemical compositions of different phases, with the detailed results depicted in Table 1. It was clear that the
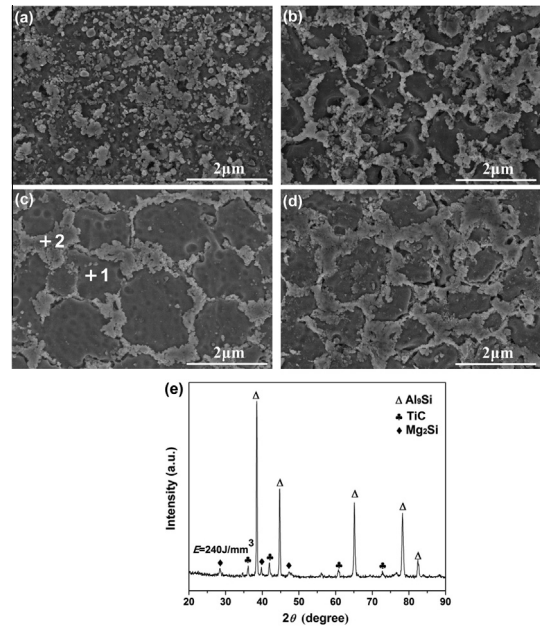
Figure 1. FE-SEM images showing typical microstructures of SLM-processed TiC/AlSi10 Mg nanocomposites at various laser energy densities (E): (a) E = 160 J mm^{-3}; (b) E = 200 J mm^{-3}; (c) E = 240 J mm^{-3}; (d) E = 280 J mm^{-3}. XRD spectra showing the constituent phases of SLM-processed Al-based nanocomposites (e).
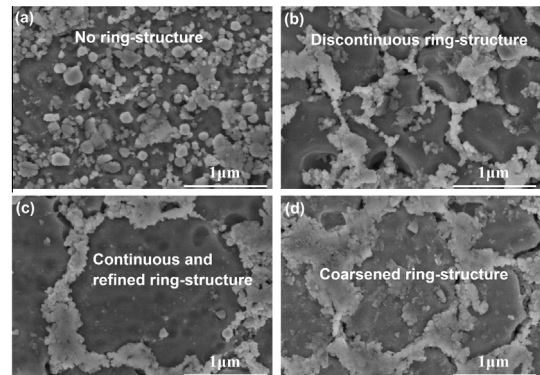
Figure 2. High-magnification FE-SEM images showing dispersion morphologies of nanoscale TiC reinforcement in SLM-processed TiC/AlSi10 Mg nanocomposites at different laser energy densities (E): (a) E = 160 J mm^{-3}; (b) E = 200 J mm^{-3}; (c) E = 240 J mm^{-3}; (d) E = 280 J mm^{-3}.

matrix was rich in Al element, with a small amount of Si, Mg, Ti and C elements dissolved inside it. The reinforcement was mainly composed of Ti and C elements with an atomic ratio very close to 1:1. The combination of XRD and EDX results revealed the formation of TiC-reinforced Al–Si–Mg-based nanocomposites after SLM.

The applied laser energy densities (E) significantly influenced the microstructural development of TiC-reinforcing phase during the SLM process. At a relatively low E of 160 J mm^{-3}, the TiC nanoparticles showed a high tendency to aggregate into inhomogeneous clusters, with some large agglomerates of TiC reinforcement formed in the matrix (Fig. 1a). High-magnification FE-SEM analysis revealed that the TiC reinforcement showed an initial particulate morphology after SLM, having a disordered distribution within the matrix (Fig. 2a). With the increase of E to 200 J mm^{-3}, the TiC reinforcement started to have a

**Table 1.** EDX results showing the chemical compositions found in different phases in Fig. 1c (at.%).

Position	Al	Si	Mg	Ti	C
Point 1, matrix	81.23	7.93	0.41	5.56	4.87
Point 2, reinforcement	5.13	0.57	0	46.64	47.66

tendency to exhibit a regular distribution, leading to the partial formation of a novel ring-structured reinforcement (Fig. 1b). When observed at a higher magnification, it was found that the TiC nanoparticles bonded with each other to form a discontinuous ring-structure (Fig. 2b). With a further increase of E to 240 J mm^{-3}, a series of ring-structured TiC reinforcements was formed along the grain boundaries of the Al-matrix in a highly homogeneous manner (Fig. 1c). High-magnification FE-SEM characterization revealed that the nanoparticles bonded with each other coherently, favoring the formation of a continuous and refined ring-structure with a mean thickness of 250 nm and an internal diameter of 2.1 μm (Fig. 2c). At an even higher E of 280 J mm^{-3}, although the regular ring-structure of TiC reinforcement was still maintained (Fig. 1d), the average thickness of the ring-structure was greatly coarsened to 490 nm due to the elevated concentration and grain growth of TiC nanoparticles (Fig. 2d). It was accordingly concluded that with the applied E optimized, the novel-structured TiC reinforcement with a refined, homogeneous ring-architecture could be tailored along the grain boundaries of the matrix in SLM-processed Al-based nanocomposites.

In the laser-induced molten pool consisting of Al melt and TiC-reinforcing particles that forms during the SLM process, the steep temperature gradient developed between the center and edge of the molten pool surface generates a surface tension gradient and resultant Marangoni flow, which in turn induces capillary forces for liquid flow [23]. When the capillary forces act on the non-spherical TiC particles, there exists a torque around the particle due to the misalignment of the particle center [24]. The present torque tends to rotate the TiC nanoparticles in the pool, providing a possibility to rearrange its distribution. It is known that the intensity of capillary forces is determined by the magnitude of the temperature gradient [22]. An insufficient laser energy input tends to weaken the SLM temperature gradient and attendant capillary force intensity, which is in turn insufficient to rearrange the TiC nanoparticles in the pool. Consequently, the distribution state of TiC reinforcing particles is considerably non-uniform at a relatively low E of 160 J mm^{-3} (Fig. 2a). When E is increased by increasing the laser power, the rearrangement rate of TiC reinforcing nanoparticles in the molten pool is elevated due to intensification of the Marangoni flow. The TiC nanoparticles are continuously driven by the torque force and gather together around the center of the Marangoni flow pattern to form the TiC ring. Meanwhile, repulsive forces tend to arise between TiC reinforcing particles when a sufficient amount of Al melt forms in the molten pool [25]. The combined effects of Marangoni flow and repulsion forces contribute to the formation of the ring-structure of TiC reinforcement in the solidified matrix when a sufficiently high E above 200 J mm^{-3} is applied (Fig. 2c). Nevertheless, with an excessive increase of E to 280 J mm^{-3}, the ring structure of TiC reinforcement shows an apparent coarsening (Fig. 2d) due to the significant thermal accumulation in the molten pool and resultant grain growth and concentration of nanoscale TiC reinforcing particles.

The influence of laser energy density (E) on the average microhardness measured on the cross-sections of SLM-processed TiC/AlSi10 Mg nanocomposite parts is depicted in Figure 3a. The average microhardness of the samples increased continuously from 157.4 HV$_{0.1}$ to 188.3 HV$_{0.1}$ with the increase in applied E from 160 to 240 J mm^{-3}. This indicated that relative to individual dispersed TiC reinforcement (Fig. 1a), the uniformly distributed ring-structures of TiC reinforcing particles along grain boundaries of the matrix (Fig. 1c) might constrain the local deformation of the matrix during indentation more efficiently, leading to an elevated hardness. However, with a further increase in E to 280 J mm^{-3}, the mean microhardness value decreased slightly to 180.6 HV$_{0.1}$, which suggested that the coarsening of the ring-structured TiC reinforcement along the grain boundaries of the matrix was detrimental to any further improvement in the microhardness. Nevertheless, it is worth noting that the SLM-processed TiC/AlSi10 Mg nanocomposite parts generally demonstrated superior hardness at all given SLM parameters as compared with the unreinforced AlSi10 Mg parts fabricated using the same SLM parameters (maximum microhardness of ~145 HV$_{0.1}$) [21].

The tensile properties (e.g. tensile strength and elongation) of TiC/AlSi10 Mg nanocomposite parts and unreinforced AlSi10 Mg parts fabricated by SLM are depicted in Figure 3b. Compared with the unreinforced AlSi10 Mg part, the tensile strength of TiC/AlSi10 Mg
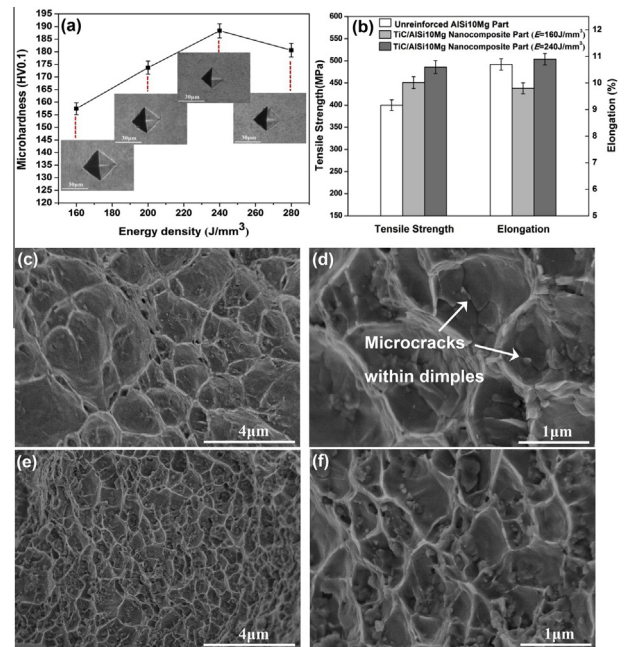
Figure 3. (a) The effect of laser energy density (E) on microhardness of SLM-processed TiC/AlSi10 Mg nanocomposite parts. (b) Tensile properties (tensile strength and elongation) of SLM-processed unreinforced AlSi10 Mg and TiC/AlSi10 Mg nanocomposite parts. FE-SEM images showing typical morphologies of fracture surfaces of SLM-processed unreinforced AlSi10 Mg (c, d) and TiC/AlSi10 Mg nanocomposite parts (e, f) at E = 240 J mm^{-3}.

nanocomposite parts at a laser energy density (E) of 160 J mm^{-3} increased from 400 to 452 MPa, whereas the elongation decreased from 10.7% to 9.8%. This thus revealed that the inhomogeneous incorporation of nano-sized TiC ceramic particles in the matrix could strengthen the Al-based composites (i.e. increase the strength), but was accompanied by a decrease in the ductility of the composites. Interestingly, with the formation of the homogeneous dispersed ring-structured TiC reinforcement along the grain boundaries of the matrix (Figs. 1c and 2c), the tensile strength of the SLM-processed TiC/AlSi10 Mg nanocomposite part at $E = 240$ J mm^{-3} increased considerably to 486 MPa, while maintaining a sufficiently high elongation (10.9%) relative to the unreinforced AlSi10 Mg alloy part. Figure 3c–f illustrates the characteristic morphologies of the fracture surfaces of the SLM-processed unreinforced AlSi10 Mg part and the TiC/AlSi10 Mg nanocomposite part with the formation of ring-structured TiC reinforcement. The fracture surfaces generally exhibited ductile-type failure, with the presence of the uniform dimples (Fig. 3c and e). Nevertheless, high-magnification FE-SEM analysis revealed some distinct differences in the fracture surface morphologies. For the unreinforced AlSi10 Mg part, dimples with a relatively large size of 2–3 μm were observed, and some microcracks were formed along grain boundaries within the dimples (Fig. 3d). For the TiC/AlSi10 Mg nanocomposite part, considerably refined dimples 0.2–0.5 μm in size were present and the ultrafine TiC reinforcing particles were uniformly incorporated in these dimples (Fig. 3f). It is accordingly reasonable to consider that the formation of novel ring-structured TiC reinforcement in SLM-processed TiC/AlSi10 Mg nanocomposites contributed to the improvement of tensile strength, while maintaining the sufficiently high ductility of the nanocomposites. This unique phenomenon is mainly attributed to the following two strengthening mechanisms:

(i) *The effect of grain refinement strengthening.* The incorporation of the nanoscale TiC reinforcing particles tends to constrain the crystalline growth of the Al matrix, thereby refining the crystal size of the finally solidified nanocomposites, as indicated by the formation of the greatly refined dimples on the fracture surface in this situation (Fig. 3e). The grain refinement effect is an efficient method for achieving a simultaneous enhancement of tensile strength and ductility [26].

(ii) *The effect of grain boundary strengthening.* With the tailored formation of the novel ring-structured TiC reinforcement after SLM (Fig. 1c), the interconnection between the neighboring TiC nanoparticles is improved (Fig. 2c) and, at the same time, the grain boundaries of the Al matrix are strengthened. During mechanical loading, the strong bonding coherence between reinforcement/matrix boundaries improves the load transfer effectively, hence increasing the tensile strength of the Al-based nanocomposites. In addition, the uniform distribution of ring-structured reinforcement along the grain boundaries can effectively constrain crack propagation during plastic deformation, which helps to enhance the ductility of the nanocomposites.

In summary, the distribution and morphology of nanoscale TiC reinforcement in an Al matrix could be tailored by controlling the laser energy density during SLM. Under the optimal laser energy density of 240 J mm^{-3}, a novel ring-structured TiC reinforcement with a regular distribution was successfully tailored. Relative to the unreinforced AlSi10 Mg alloy part prepared under the same SLM conditions, the TiC/AlSi10 Mg nanocomposites with this novel reinforcement architecture exhibited elevated microhardness (188.3 HV$_{0.1}$) and tensile strength (486 MPa) without any reduction in elongation (10.9%).

[1] P.B. Kadolkar, T.R. Watkins, J.Th.M. De Hosson, B.J. Kooi, N.B. Dahotre, Acta Mater. 55 (2007) 1203.
[2] J.A. Vreeling, V. Ocelƚk, G.A. Hamstra, Y.T. Pei, J. Th.M. De Hosson, Scripta Mater. 42 (2000) 589.
[3] R. Anandkumar, A. Almeida, R. Colaço, R. Vilar, V. Ocelik, J.Th.M. De Hosson, Surf. Coat Technol. 201 (2007) 9497.
[4] B. Torres, M. Lieblich, J. Ibáñez, A. García-Escorial, Scripta Mater. 47 (2002) 45.
[5] S.C. Tjong, Adv. Eng. Mater. 9 (2007) 639.
[6] H.R. Ezatpour, S.A. Sajjadi, M.H. Sabzevar, Y.Z. Huang, Mater. Sci. Eng. A 607 (2014) 589.
[7] A. AnsaryYar, M. Montazerian, H. Abdizadeh, H.R. Baharvandi, J. Alloys Compd. 484 (2009) 400.
[8] V. Viswanathan, T. Laha, K. Balani, A. Agarwal, S. Seal, Mater. Sci. Eng. R 54 (2006) 121.
[9] W.J. Kim, Y.J. Yu, Scripta Mater. 72–73 (2014) 25.
[10] H. Arami, A. Simchi, S.M. Seyed, Reihani, J. Alloys Compd. 465 (2008) 151.
[11] S.D. Luo, Q. Li, J. Tian, C. Wang, M. Yan, G.B. Schaffer, M. Qian, Scripta Mater. 69 (2013) 29.
[12] J.Y. Wang, Z.Q. Li, G.L. Fan, H.H. Pan, Z.X. Chen, D. Zhang, Scripta Mater. 66 (2012) 594.
[13] L.J. Huang, L. Geng, A.B. Li, F.Y. Yang, H.X. Peng, Scripta Mater. 60 (2009) 996.
[14] H.X. Peng, Z. Fan, J.R.G. Evans, Mater. Sci. Eng. A 303 (2001) 37.
[15] L.C. Zhang, D. Klemm, J. Eckert, Y.L. Hao, T.B. Sercombe, Scripta Mater. 65 (2011) 21.
[16] B. Song, S.J. Dong, C. Coddet, Scripta Mater. 75 (2014) 90.
[17] D.D. Gu, G.B. Meng, C. Li, W. Meiners, R. Poprawe, Scripta Mater. 67 (2012) 185.
[18] M. Das, V.K. Balla, D. Basu, S. Bose, A. Bandyopadhyay, Scripta Mater. 63 (2010) 438.
[19] Y.T. Pei, V. Ocelik, J.Th.M. De Hosson, Acta Mater. 50 (2002) 2035.
[20] Y.T. Pei, J.Th.M. De Hosson, Acta Mater. 48 (2000) 2617.
[21] E. Brandl, U. Heckenberger, V. Holzinger, D. Buchbinder, Mater. Des. 34 (2012) 159.
[22] D.D. Gu, W. Meiners, K. Wissenbach, R. Poprawe, Int. Mater. Rev. 57 (2012) 133.
[23] J.P. Kruth, G. Levy, F. Klocke, T.H.C. Childs, CIRP Ann. Manuf. Technol. 56 (2007) 730.
[24] H.J. Niu, I.T.H. Chang, Scripta Mater. 41 (1999) 25.
[25] L.A. Anestiev, L. Froyen, J. Appl. Phys. 86 (1999) 4008.
[26] K. Lu, Science 328 (2010) 319.